TABLE 2 Molar conductances of KCl in H_2O–D_2O at 25 °C

C (mol dm^{-3})	X_D 0	0.5	1
0.1	129.02	117.31	107.48
0.05	133.43	121.23	110.73
0.01	141.33	128.23	117.19
$C \to 0$	150.0	136.06	124.3
$\Delta\Lambda(X_D, C \to 0)$	—	−1.09	—
$\Delta^{rel}(X_D, C \to 0)$	—	−0.8%	—

See Table 1 notes for explanations.

This experiment was proposed[9] as a critical test of a theoretical prediction concerning the possible existence of quantum correlations between H^+ and protons of water molecules[3,9]. This hypothesis was motivated by the detailed analysis of Hertz[21] concerning the impossibility of directly deducing (from any known experiment) the existence of H^+ as a well defined particle in aqueous solutions, and by the classic work of Eigen[1,2] concerning the quantum tunnelling of protons in H_2O clusters.

In the framework of our general theory of quantum correlations[8], the interpretation of the anomalous conductance is based on the following point[9]. If the well-known high H^+ conductance, λ_{H^+}, in liquid water is caused by the assumed specific quantum interference and delocalization effect (the coherent dissipative structures[3,8]) then there must be an anomalous decrease of λ_{H^+} in H_2O–D_2O mixtures owing to the mass and spin 'superselection rules'[4]. In these mixtures, the quantum interference between appropriate proton states becomes disrupted by deuterons 'belonging to' D_2O, HDO or D^+ ions and being 'near' or 'between' the considered protons. This implies that the spatial extension of the corresponding coherent dissipative structures (which describe the delocalization of the protons participating in them) becomes restricted, causing a corresponding decrease of λ_{H^+}. (The same conclusion holds for the D^+ conductance; see, however, ref. 3). In general, quantum correlations have no classical analogue[4–6,8], so there are no 'molecular pictures' of these structures.

Our observations suggest that this effect may play an important part in the dynamics of proton transfer and hydrogen-bond formation[22] in other physical, chemical and biological systems. Further work is in progress. □

Received 5 March; accepted 6 June 1990.

1. Eigen, M. & de Maeyer, L. *Proc. R. Soc.* A**247,** 505–533 (1958).
2. Eigen, M. *Angew. Chem.* **75,** 489–508 (1963), English translation, *Angew. Chem. int. Ed.* **3,** 1–19 (1964).
3. Chatzidimitriou-Dreismann, C. A. & Brändas, E. J. *Int. J. Quantum Chem.* **37,** 155–165 (1990).
4. Primas, H. *Chemistry, Quantum Mechanics and Reductionism* (Springer, Berlin, 1983).
5. d'Espagnat, B. *Phys. Rep.* **110,** 201–264 (1984).
6. d'Espagnat, B. *Conceptual Foundations of Quantum Mechanics* 2nd edn (Addison–Wesley, Redwood City, 1989).
7. Einstein, A., Podolsky, B. & Rosen, N. *Phys. Rev.* **47,** 777–780 (1935).
8. Brändas, E. J. & Chatzidimitriou-Dreismann, C. A. in *Resonances* (eds Brändas, E. & Elander, N.) Lecture Notes in Physics, Vol. 325, 485–540 (Springer, Berlin, 1989).
9. Chatzidimitriou-Dreismann, C. A. *Int. J. Quantum Chem., Symp.* **23,** 153–158 (1989).
10. Stokes, R. H. *J. phys. Chem.* **65,** 1242–1247 (1961).
11. Haase, R., Sauerman, P. F. & Dücker, K. H. *Z. phys. Chem.* **47,** 224–245 (1965).
12. Kell, G. S. *J. chem. Ref. Data* **6,** 1109 (1977).
13. Longsworth, L. G. *J. phys. Chem.* **64,** 1914–1917 (1960).
14. Robinson, R. A. & Stokes, R. H. *Electrolyte Solutions* (Butterworths, London, 1970).
15. Frivold, O. E., Hassel, O. & Hetland, E. *Avhandl. Norske Videnskaps Akad. Oslo I Mat. Naturv. Kl.* No. 9, 1 (1942).
16. *Gmelin's Handbuch der Anoganischen Chemie, Chlor,* Suppl. Issue Part B1, 8 edn (Verlag-Chemie, Weinheim, 1969).
17. Longsworth, L. G. & McInnes, D. A. *J. Am. chem. Soc.* **59,** 1666–1670 (1937).
18. Swain, D. G. & Evans, D. F. *J. Am. chem. Soc.* **88,** 383–390 (1966).
19. Jones, G. & Fornwald, H. *J. chem. Phys.* **4,** 30–33 (1936).
20. Weingärtner, H. *Ber. Bunsenges. phys. Chem.* **88,** 47–50 (1984).
21. Hertz, H. G. *Chem. Scripta* **27,** 479–493 (1987).
22. Zundel, G. & Eckert, M. *J. molec. Struct.* **200,** 73–92 (1989).

ACKNOWLEDGEMENTS. We thank G. Ertl for discussions and for suggesting this experiment, E. Brändas and G. Hertz for discussions, and U. Schneider for assistance in some of the measurements. This work was supported by the Commission of the European Communities, the Deutsche Forschungsgemeinschaft and the Fonds der Chemischen Industrie.

High-resolution ^{27}Al NMR spectroscopy of the aluminophosphate molecular sieve VPI-5

Y. Wu*, B. F. Chmelka*, A. Pines*§, M. E. Davis†, P. J. Grobet‡ & P. A. Jacobs‡

* Materials and Chemical Sciences Division, Lawrence Berkeley Laboratory, 1 Cyclotron Road, Berkeley, California 94720 and Department of Chemistry, University of California, Berkeley, California 94720, USA
‡ Department of Chemical Engineering, Virginia Polytechnic Institute and State University, Blacksburg, Virginia 24061, USA
§ Laboratorium voor Oppervlaktechemie, Catholic University of Leuven, B-3030 Leuven, Belgium

ALUMINIUM plays an important part in determining the properties of many materials, such as the catalytic behaviour of zeolites. Aluminophosphate molecular sieves, in particular, have useful applications as superlattice hosts in the fabrication of quantum-effect devices[1]. Although nuclear magnetic resonance (NMR) spectroscopy is often a sensitive probe of solids, the use of ^{27}Al NMR to investigate the structure of aluminosilicates and aluminophosphates has been severely limited because anisotropic second-order quadrupolar interactions, responsible for spectral broadening, cannot be eliminated by conventional magic-angle-spinning or multiple-pulse techniques. Here we report the first high-resolution NMR spectra of ^{27}Al in a solid using double rotation[2–4] and demonstrate its usefulness for probing subtle structural perturbations in the aluminophosphate molecular sieve VPI-5[5,6]. From our results, we conclude that high-resolution ^{27}Al NMR is capable of resolving discrete framework aluminium sites, permitting quantitative investigation of site-specific adsorbate interactions with the VPI-5 host.

VPI-5 is a hydrophilic molecular sieve belonging to the aluminophosphate ($AlPO_4$) family. The proposed structure of VPI-5 in Fig. 1, based on X-ray and neutron powder diffraction experiments[5–8], consists of alternating AlO_4 and PO_4 tetrahedral units arranged to produce linear channels 12 Å in diameter. There are two crystallographically distinct aluminium sites: one located between the two four-membered rings (Al-1 in Fig. 1) and the other situated in the six-membered rings (Al-2). The ratio of the number of Al-1 to Al-2 sites is 1 : 2, and the hexagonal unit-cell parameters a and c are 19.009 Å and 8.122 Å, respectively, in the hydrated material. On dehydration, structural changes result in a contraction of a to 18.549 Å and an expansion of c to 8.404 Å (ref. 7). Such local perturbations in the framework lead to changes in chemical shifts and quadrupole interactions of the ^{27}Al nucleus. In a resolved NMR spectrum the isotropic chemical shift δ, the quadrupole-coupling constant ν_Q and the asymmetry parameter η should provide information about the symmetry and structure at the aluminium sites in the aluminophosphate framework.

We carried out ^{27}Al NMR experiments in a pulsed spectrometer operating at 104.23 MHz using a standard magic-angle-spinning (MAS) probe as well as a newly developed double-rotation (DOR) probe[9]. Figure 2*a* shows the ^{27}Al MAS spectrum of hydrated, polycrystalline VPI-5 spinning at 5 kHz. As observed previously[8,10], it contains an asymmetric peak at ~41 p.p.m. and a second peak below 0 p.p.m. The resonance at 41 p.p.m. falls in the range of isotropic shifts attributed to tetrahedrally coordinated Al sites, Al(IV), whereas the peak below 0 p.p.m. is attributed to octahedrally coordinated Al sites, Al(VI) (ref. 11). Figure 2*b* shows the DOR spectrum of the same hydrated sample of VPI-5. Two peaks, a and b, of equal

§ To whom correspondence should be addressed.

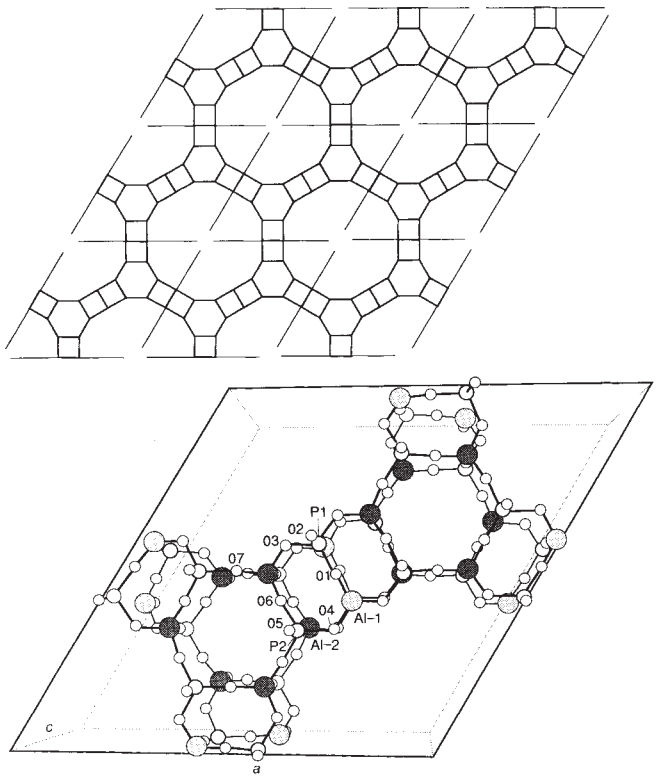

FIG. 1 The VPI-5 framework structure. Top, [001] projection, where the black lines represent oxygen atoms bonded to aluminium and phosphorus atoms at the vertices. Bottom, Hexagonal unit cell with labelled atoms.

intensity and with 1-p.p.m. linewidths at 41.2 and 40.4 p.p.m., are partially resolved, as well as a single peak, c, at −18.4 p.p.m. The intensities of the peaks are in a 1:1:1 ratio, so peak c at −18.4 p.p.m. apparently originates from half of the Al-2 sites which chemisorb water to acquire octahedral coordination as Al-2(VI). The remaining Al-2(IV) sites and all of the Al-1(IV) sites produce the two partially resolved peaks near 41 p.p.m. Peaks a and b have quite different quadrupole interaction parameters (Y.W. *et al.*, manuscript in preparation), consistent with their assignment to the different framework aluminium positions. One cannot, however, rule out the possibility that Al-1 sites become octahedrally coordinated during hydration, distorting the lattice and rendering the Al-2 sites inequivalent. VPI-5 can contain up to ~24 wt% water ($AlPO_4 \cdot 2.3H_2O$) in the fully hydrated state, indicating that both chemisorption ($Al(IV) \rightarrow Al(VI) : AlPO_4 \cdot 0.67H_2O$) and physisorption of water occur.

Figure 3*a*, *b* shows the ^{27}Al MAS spectrum for VPI-5 spinning at 5 kHz and the ^{27}Al DOR spectrum of the same sample, both acquired immediately after room-temperature dehydration for 48 h at 10^{-5} torr. Two peaks unresolved in the MAS spectrum, d at 33.3 p.p.m. and e at 35.9 p.p.m., are observed in the DOR spectrum. From the 1:2 intensity ratio of these two peaks, peak d is assigned to Al-1 sites and peak e is attributed to Al-2 sites, both of which represent tetrahedrally coordinated aluminium. During dehydration, Al(VI) sites are converted into Al(IV) sites, consistent with the disappearance of peak c at −18.4 p.p.m. Furthermore, in hydrated VPI-5, ^{27}Al tetrahedral sites (peaks a and b) are altered by dehydration to yield different ^{27}Al tetrahedral environments (peaks d and e). The weak peak f at 22.8 p.p.m. may arise from partial hydration of Al sites coordinated

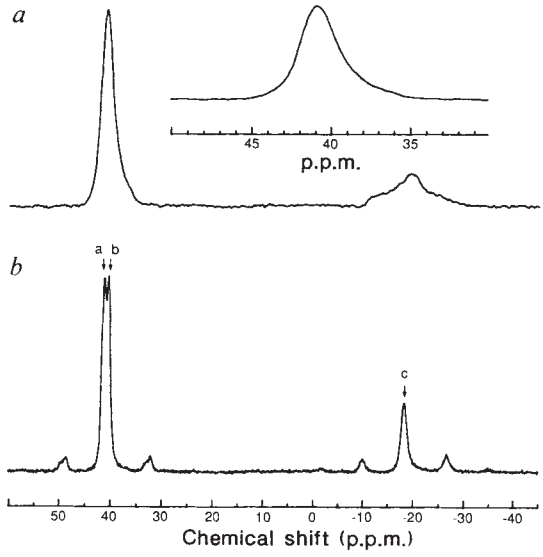

FIG. 2 ^{27}Al NMR spectra of hydrated VPI-5 under conditions of magic-angle spinning (*a*) and double rotation (*b*). Peaks not indicated by arrows are spinning sidebands. Isotropic DOR peak positions reflect contributions from both the isotropic chemical shift and the isotropic second-order quadrupole shift. Spectra are referenced to dilute aqueous $Al(NO_3)_3$.

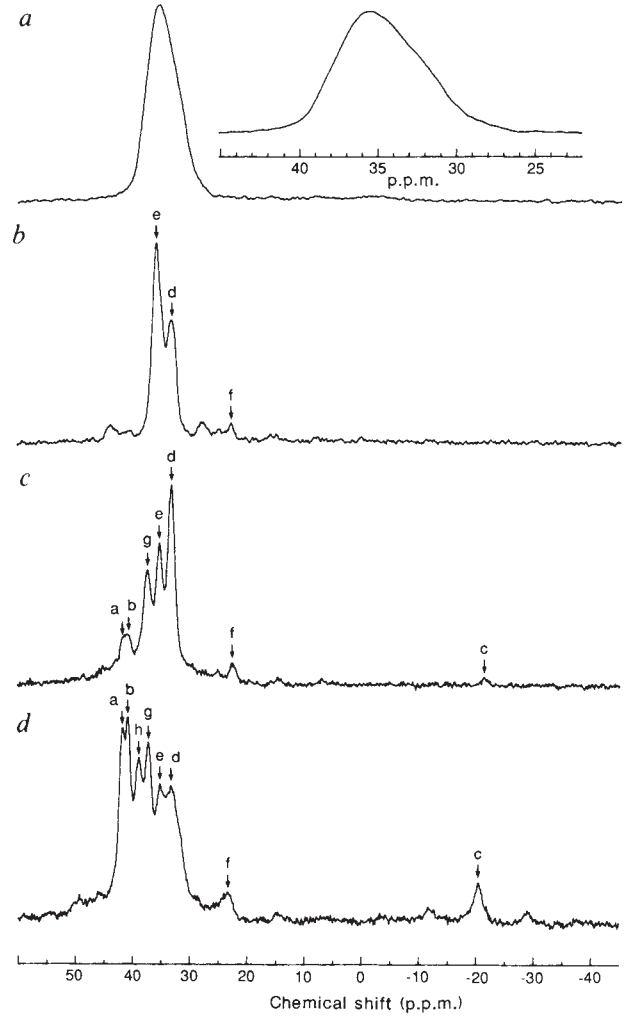

FIG. 3 ^{27}Al NMR spectra of dehydrated and partially rehydrated VPI-5. *a*, MAS spectrum of dehydrated VPI-5. *b*, DOR spectrum of dehydrated VPI-5. *c*, DOR spectrum after two days of rehydration. *d*, DOR spectrum after 23 days of rehydration. Spectra are referenced to dilute aqueous $Al(NO_3)_3$ and are plotted on arbitrary intensity scales.

to one water molecule. Figure 3*c*, *d* shows ^{27}Al DOR spectra taken 2 days and 23 days after dehydration; the sample remained inside the inner rotor of the DOR probe during this period, allowing water molecules to diffuse slowly into the material. The two sharp lines that emerge, g at 37.3 p.p.m. and h at 38.8 p.p.m., arise from Al-2 species influenced by adsorbed water molecules. Figure 3*c* shows that the relative intensity of peak d associated with dehydrated Al-1 sites undergoes little change as a result of partial rehydration, bearing in mind that the 1:2 ratio of Al-1 to Al-2 species must be maintained at all stages of hydration. The sensitivity of the VPI-5 framework to guest loading and packing, as indicated by these data, should yield new insight into the behaviour of molecules in confined microporous environments.

Both DOR and dynamic angle spinning (DAS) (recently demonstrated for ^{17}O and ^{23}Na (ref. 12)) make it possible to measure ^{27}Al quadrupole-coupling parameters and chemical shifts, allowing the study of adsorbate–host interactions in molecular sieves and subtle microstructural features in other aluminium-containing solids including catalysts, glasses, ceramics, minerals and semiconductors. □

Received 3 April; accepted 4 June 1990.

1. Stucky, G. D. & MacDougall, J. E. *Science* **247,** 669–678 (1990).
2. Llor, A. & Virlet, J. *Chem. Phys. Lett.* **152,** 248–253 (1988).
3. Samoson, A., Lippmaa, E. & Pines, A. *Mol. Phys.* **65,** 1013–1018 (1988).
4. Chmelka, B. F. *et al. Nature* **339,** 42–43 (1989).
5. Davis, M. E., Saldarriaga, C., Garces, J. M. & Crowder, C. *Nature* **331,** 698–699 (1988).
6. Crowder, C. E., Garces, J. M. & Davis, M. E. *Adv. X-ray Analysis* **32,** 503–510 (1989).
7. Richardson, J. W. Jr, Smith, J. V. & Pluth, J. J. *J. phys. Chem.* **93,** 8212–8219 (1989).
8. Davis, M. E. *et al. J. Am. chem. Soc.* **111,** 3919–3924 (1989).
9. Wu, Y., Sun, B. Q., Pines, A., Samoson, A. & Lippmaa, E. *J. magn. Res.* (in the press).
10. Grobet, P. J. *et al. Appl. Catal.* **56,** L21–L27 (1989).
11. Blackwell, C. S. & Patton R. L. *J. phys. Chem.* **88,** 6135–6139 (1984).
12. Mueller, K. T. *et al. J. magn. Res.* **86,** 470–487 (1990).

ACKNOWLEDGEMENTS. This work was supported by the Office of Basic Energy Sciences, Materials and Chemical Sciences Division, US Department of Energy and by the Shell Foundation. The authors thank J. A. Martens for assistance with VPI-5 sample preparation. B.F.C. is a NSF post-doctoral fellow.

Importance of biomass burning in the atmospheric budgets of nitrogen-containing gases

Jürgen M. Lobert, Dieter H. Scharffe, Wei M. Hao & Paul J. Crutzen

Department of Atmospheric Chemistry, Max-Planck-Institut für Chemie, PO Box 3060, 6500 Mainz, FRG

BIOMASS burning is a primary source of many trace substances that are important in atmospheric chemistry[1–6]. More than 80% of the world's biomass burning takes place in the tropics[3] as a result of savanna fires, forest-clearing activity, and the burning of agricultural waste and wood. Here we report results from laboratory studies on the emission of nitrogen-containing compounds from the burning of dry vegetation. We find that the emission rates of NO_x, HCN and CH_3CN are sufficient to contribute significantly to the global atmospheric budget of the compounds. Furthermore, possibly up to half of the biomass nitrogen can be converted to molecular nitrogen, N_2, leading to an estimated annual loss of $12–28 \times 10^{12}$ g of biomass nitrogen ('pyrodenitrification'), equal to ~9–20% of the estimated global rate of terrestrial nitrogen fixation.

According to recent estimates[3], $\sim 3–6 \times 10^{15}$ g of biomass carbon is burned annually, corresponding to $24–57 \times 10^{12}$ g of biomass nitrogen. This burning produces mostly CO_2, but also 10% CO and ~2% CH_4 and other hydrocarbons. Many other gases and particulate matter are also emitted. Here we consider the emissions of nitrogen-containing compounds.

Our results have been obtained using a small-scale burning apparatus built to simulate open fires (Fig. 1). The details of this apparatus are described elsewhere[6]. Because most of the biomass burning takes place in the tropics, we burned mostly tropical grasses from savanna regions and also agricultural wastes, in a total of 41 burning experiments.

Our analytical system was designed to determine CO_2, CO, non-methane hydrocarbons (NMHC) and CH_4 as well as the most important nitrogen-containing species: NO_x (NO and NO_2), ammonia (NH_3), some cyanogen compounds such as hydrogen cyanide (HCN) and acetonitrile (CH_3CN), and nitrous oxide (N_2O). Determination of the flow rate in the stack, the weight loss of the fuel, and the elemental content of both biomass and ash, as well as the concentrations of gaseous emissions, enabled us to carry out a mass balance for each experiment.

Our apparatus also allows us to observe the different burning stages separately. A burn can be divided into a hot flaming phase emitting oxidized compounds such as CO_2, NO_x and N_2O, and a colder, incompletely combusting smouldering phase producing much more smoke and less oxidized substances such as CO, hydrocarbons, ammonia and nitriles[6]. Figure 2 shows some of the compounds emitted during one of our experiments, and the corresponding stack-gas temperature. The transition between flaming and smouldering combustion is clearly observable in our experiments and corresponds to a large increase in the CO concentration and a decrease in CO_2 emission at ~96 s.

Our data show that on average ~90% of the biomass nitrogen and 95% of the carbon were volatilized during the burn, with a mean weight loss of 75% in the flaming and 25% in the smouldering stage. Almost all of the carbon was recovered in the measured emissions of CO_2, CO, hydrocarbons and in the ash. By contrast, only ~32% of the nitrogen could be regained by the above mentioned nitrogen-containing compounds and the nitrogen content of the ash (Table 1).

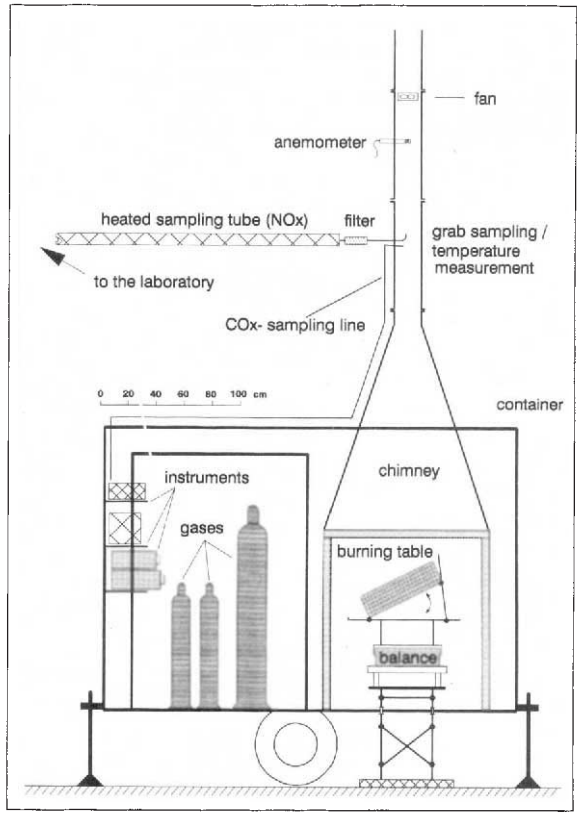

FIG. 1 Burning apparatus for an experimental simulation of open biomass burning[6].